iScience

Article

Lumbar spinal Shox2 interneurons receive monosynaptic excitatory input from the lateral paragigantocellular nucleus in mouse

Graphical abstract

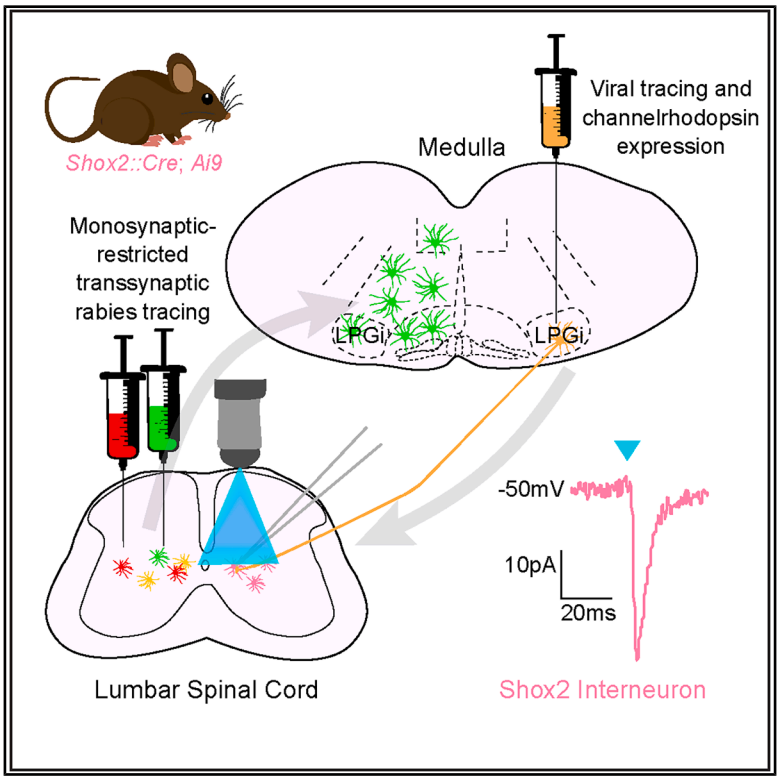

Highlights

- Several brainstem nuclei make direct connections to lumbar Shox2 interneurons
- Monosynaptic connections include glutamatergic LPGi neurons to Shox2 interneurons
- Functional excitatory reticulospinal to Shox2 interneuron connections demonstrated

Authors

Shayna Singh, Lihua Yao, Kimberly J. Dougherty

Correspondence

kjd86@drexel.edu

In brief

Cellular neuroscience; Molecular neuroscience; Neuroscience

Singh et al., 2026, iScience 29, 114567
February 20, 2026
https://doi.org/10.1016/j.isci.2025.114567

CellPress

iScience

CellPress
OPEN ACCESS

Article

Lumbar spinal Shox2 interneurons receive monosynaptic excitatory input from the lateral paragigantocellular nucleus in mouse

Shayna Singh,[1] Lihua Yao,[1] and Kimberly J. Dougherty[1,2,*]
[1]Marion Murray Spinal Cord Research Center, Department of Neurobiology and Anatomy, Drexel University College of Medicine, Philadelphia, PA 19129, USA
[2]Lead contact
*Correspondence: kjd86@drexel.edu
https://doi.org/10.1016/j.isci.2025.114567

SUMMARY

Locomotion in vertebrates is generated in the spinal cord but initiated by supraspinal centers. Spinal interneurons expressing Shox2 include putative locomotor rhythm generating neurons in mice. Reticulospinal neurons directly provide drive to spinal rhythm generating interneurons, which then convey rhythmic output. Excitatory neurons in the lateral paragigantocellular nucleus (LPGi) have been shown to provide this descending drive during locomotor initiation. Here, we performed viral tracing and electrophysiology to test for direct connections between the LPGi and lumbar Shox2 interneurons in adult mice. Using monosynaptic-restricted rabies tracing, we show that excitatory neurons from the LPGi make direct synaptic connections onto lumbar Shox2 interneurons. This connection from the ventral caudal medulla to Shox2 interneurons was confirmed via anterograde tracing and recordings of excitatory postsynaptic potentials in Shox2 interneurons. Thus, a subset of Shox2 interneurons receives monosynaptic excitatory input from the LPGi, which may provide the substrate for locomotor initiation.

INTRODUCTION

Locomotion is one of the primary ways by which vertebrates dynamically interact with their environments. Locomotion in vertebrates is initiated by neural circuitry spanning the entire central nervous system. A number of genetically identified populations of spinal interneurons have been shown to contribute to various aspects of locomotion.[1,2] Among these, Shox2 interneurons are a putative rhythm-generating population of excitatory neurons located ventromedially in the spinal cord[3] exhibiting many of the criteria for rhythmogenic locomotor-related neurons.[4] Although there are other populations proposed to contribute to rhythm generation, including the Hb9 interneurons,[4–6] Lhx9 interneurons,[7] and ventral spinocerebellar tract (VSCT) neurons,[8] the location, electrophysiological properties, and local connectivity of the Shox2 interneurons is most consistent with a primary role in rhythm generation.[3,9,10] However, the supraspinal structures targeting these neurons are yet unknown.

Rhythm generating neurons are hypothesized to receive an initiation signal from supraspinal structures, which is converted to a rhythmic motor output.[4,11–14] The reticulospinal tract has long been suggested to serve as a direct link between supraspinal effectors and spinal interneurons in the context of motor output.[15] The descending reticulospinal drive originating in the medulla acts as a necessary intermediary between the mesencephalic locomotor region and the spinal locomotor central pattern generator.[13,16,17] In freely behaving mice, targeted activation within medullary reticulospinal nuclei initiates,[18] halts,[18,19] or redirects/turns[19,20] locomotion. Similarly, glutamatergic reticulospinal transmission generates rhythmic locomotor-like behavior *in vitro*.[11] Reticulospinal projections have been shown to directly contact commissural interneurons[21–23] and motor neurons.[24] However, a determination of relation to function is complicated by the diversity in both the medullary nuclei that form the reticular spinal pathway and spinal interneuron populations.

Higher specificity has been gained more recently. Using either anterograde or retrograde viral tracing strategies from specified interneuronal populations, the gigantocellular nucleus has been shown to project to a variety of spinal neurons. These include lumbar V2a interneurons[25] involved in left-right co-ordination[26,27] and functional recovery following SCI,[25] lumbar Dmrt3 commissural neurons that participate in left-right alternation,[28] and cervical V1 interneurons[29] that mediate flexor/extensor co-ordination and locomotor speed.[30,31] It is notable that direct reticulospinal input to these or other populations of locomotor-related lumbar spinal neurons has rarely been functionally assessed.

The lateral paragigantocellular nucleus (LPGi) has been implicated in the initiation of forward locomotion from rest.[18] Specifically, activation of glutamatergic LPGi neurons drives locomotion *in vivo*.[18] The speed of this excitatory LPGi-driven locomotor behavior was shown to scale with activation intensity,[18] suggesting that excitatory LPGi neurons have robust access to the spinal circuitry, which dictates locomotor rhythm. Further, reticulospinal

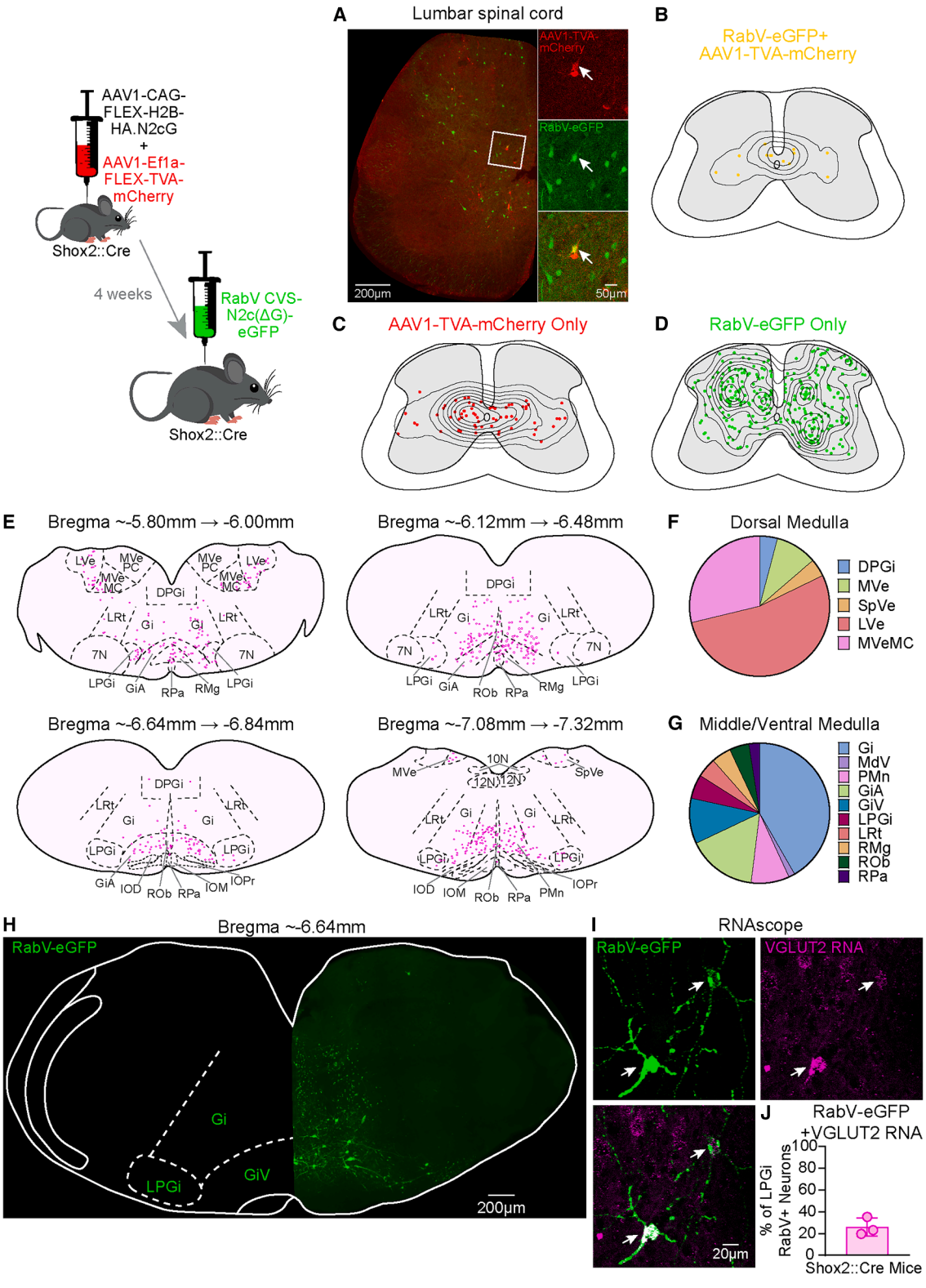

(legend on next page)

terminations from LPGi and neighboring caudal ventrolateral reticular nucleus forming a "hot spot" for the initiation of locomotor-like activity in the spinal cord are highly dense in medial lamina VII,[32,33] consistent in location to be in overlap with lumbar Shox2 interneurons.

The reticulospinal tract has been the subject of studies aiming to improve motor function after spinal cord injury[25,34–36] so that the identification of the specific connections made by the reticulospinal tract with spinal interneurons can be targeted in efforts to restore locomotor function after injury. Thus, our goal was to test the hypothesis that excitatory LPGi neurons make functional synaptic connections with lumbar Shox2 interneurons. We demonstrate a direct connection between excitatory neurons originating in the LPGi and lumbar spinal Shox2 interneurons in adult mice using retrograde transsynaptic tracing. We show, both anatomically and electrophysiologically, that a subset of lumbar spinal Shox2 interneurons receives excitatory monosynaptic input from reticulospinal neurons in the ventral caudal medulla, providing evidence for a potential pathway for the initiation of locomotion.

RESULTS

Transsynaptic viral-mediated tracing demonstrates a monosynaptic connection between the LPGi and Shox2 interneurons

It has been previously propounded that locomotor-related rhythmogenic spinal interneurons should receive supraspinal drive via direct excitatory reticulospinal input.[4,11–14] To determine whether a monosynaptic connection was present between the LPGi and lumbar spinal Shox2 interneurons, we performed monosynaptic-restricted transsynaptic tracing with the CVS-N2c(ΔG) strain[37] of rabies virus (RabV CVS-N2c[ΔG]-eGFP). This strategy has previously been employed to study V1 interneurons in the cervical spinal cord.[29] We simultaneously injected two Cre-dependent AAVs into the lumbar spinal cord of adult *Shox2::Cre* mice to generate the expression of the necessary glycoprotein (N2cG) for rabies transsynaptic transmission, and the necessary cellular receptor TVA for EnvA-dependent rabies virus-host membrane fusion. We then injected CVS-N2c(ΔG) rabies virus (RabV) into the same site in the lumbar spinal cord 4 weeks later. We found RabV-eGFP$^+$/AAV1-TVA-mCherry$^+$ starter cells (Figures 1A and 1B) and cells which were only AAV1-TVA-mCherry$^+$ (Figure 1C), which were restricted to the ventromedial lumbar spinal cord where Shox2 interneurons reside (N = 3 mice). However, cells which were only RabV-eGFP$^+$ extended throughout the dorsal horn in the lumbar spinal cord as well (Figure 1D).

We mapped RabV-eGFP$^+$ neurons in sections containing the reticulospinal nuclei from the medulla (Figure 1E). We found eGFP$^+$ neurons in the middle and ventral medulla (n = 473 neurons, N = 3 mice), including in the LPGi, gigantocellular nucleus (Gi), ventral gigantocellular nucleus (GiV), anterior gigantocellular nucleus, the medullary reticular formation ventral part, the paramedian reticular nucleus, the lateral reticular nucleus, and several raphe nuclei (Figures 1E and 1F). Dorsal medullary nuclei also contained RabV-eGFP$^+$ cells (n = 55 neurons, N = 3 mice), including the dorsal paragigantocellular nucleus and various vestibular nuclei (Figures 1E and 1G).

We then focused on the LPGi neurons, which monosynaptically contact lumbar spinal Shox2 interneurons (Figure 1H). We performed RNAscope (Figure 1I), which revealed that a subset (22%) of eGFP$^+$ neurons in the LPGi which monosynaptically contact lumbar spinal Shox2 interneurons contain vesicular glutamate transporter 2 (VGLUT2) RNA (Figure 1J). Although the excitatory neurons may be underestimated due to bias of the RabV or underdetection of VGLUT2 RNA, this demonstrates that excitatory neurons in the LPGi are monosynaptically connected to lumbar spinal Shox2 interneurons.

We performed control experiments in age-matched wild-type mice, which do not express Cre. Injections of only RabV-eGFP (Figure S1A) or AAV1-CAG-FLEX-H2B-HA.N2cG, AAV1-Ef1a-FLEX-TVA-mCherry, and RabV-eGFP (Figure S1B) resulted in no fluorescently labeled cells in either the spinal cord or in the medullary nuclei. Any fluorescence detected in these images was auto-fluorescence and was equally intense in all testable channels. Cell counts from experimental and control injections in all examined regions are compiled in Table S1. Taken together, these data demonstrate that lumbar spinal Shox2 interneurons receive monosynaptic connections from many medullary nuclei and spinal cord cells, including excitatory LPGi neurons.

Figure 1. Transsynaptic rabies tracing from lumbar spinal Shox2 interneurons reveals starter cells and monosynaptically connected cells

(A) Representative image following bilateral microinjections of helper AAVs, AAV1-CAG-FLEX-H2B-HA.N2cG and AAV1-Ef1a-FLEX-TVA-mCherry, and RabV CVS-N2c(ΔG)-eGFP showing RabV-eGFP$^+$ cells (green), AAV1-TVA-mCherry$^+$ cells (red), and RabV-eGFP$^+$/AAV1-TVA-mCherry$^+$ starter cells (yellow) present in the lumbar spinal cord. Scale bars, 200 μm (left) and 50 μm (right).

(B) Density contour plot of mapped RabV-eGFP$^+$/AAV1-TVA-mCherry$^+$ starter cell bodies.

(C) Density contour plot of mapped AAV1-TVA-mCherry$^+$ cell bodies.

(D) Density contour plot of mapped RabV-eGFP$^+$ cell bodies.

(E) Representative maps of cell body positions of RabV-eGFP$^+$ cells from images matched to atlas figures to define nuclei boundaries.

(F) Relative distribution of RabV-eGFP$^+$ cells within nuclei in the dorsal medulla. Data represent the proportion of the total eGFP+ cell count in the dorsal medulla.

(G) Relative distribution of RabV-eGFP$^+$ cells within nuclei in the middle and ventral medulla. Data represent the proportion of the total eGFP$^+$ cell count in the middle and ventral medulla.

(H) eGFP$^+$ cells in the medulla (green) at approximately Bregma −6.64. Scale bars, 200 μm.

(I and J) Cell counts in the LPGi after probing for eGFP RNA and VGLUT2 RNA using RNAscope demonstrates that approximately 22% of eGFP RNA$^+$ cells (green) are also VGLUT2 RNA$^+$ (magenta). Scale bars, 20 μm. N = 3 mice.

DPGI, dorsal paragigantocellular nucleus; MVe, medial vestibular nucleus; SpVe, spinal vestibular nucleus; LVe, lateral vestibular nucleus; MVeMC, medial vestibular nucleus magnocellular part; Gi, gigantocellular nucleus; MdV, ventral medial reticular nucleus; PMn, paramedian reticular nucleus; GiA, anterior gigantocellular nucleus; GiV, ventral gigantocellular nucleus; LPGi, lateral paragigantocellular nucleus; LRt, lateral reticular nucleus; RMg, raphe magnus; ROb, raphe obscuris; RPa, raphe pallidus.[38] See also Figure S1 and Table S1.

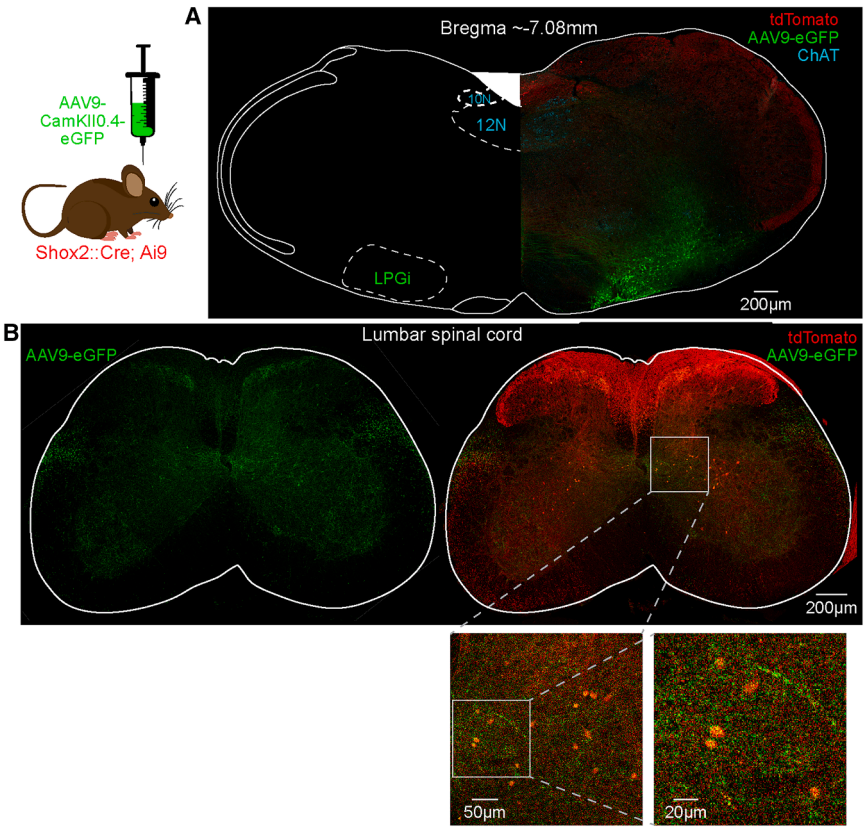

Figure 2. Anterograde viral tracing of spinal projections

(A) Bilateral injections of AAV9-CamKII0.4-eGFP-WPRE-rBG were delivered to adult *Shox2::Cre*; *Ai9(RCL-tdT)* mice, resulting in fluorescently labeled cell bodies in the LPGi (green) at the level of the ChAT$^+$ 10th and 12th cranial nerve motor nuclei (cyan) at approximately −7.08 from Bregma.[38]

(B) eGFP$^+$ projections in the lumbar spinal cord (green) overlap with the ventromedial location of Shox2 interneurons (red). Scale bars, 200 μm. Insets display the boxed region at a higher magnification. Left inset, scale bar, 50 μm; right inset, scale bar, 20 μm. *N* = 4 mice.

Anterograde viral-mediated tracing demonstrates a connection between excitatory reticulospinal neurons and Shox2 interneurons

To validate the connection between the LPGi and lumbar spinal Shox2 interneurons, anterograde viral-mediated tracings were performed. This strategy efficiently labels the LPGi and reveals the connections to all spinal neurons, not specifically to the Shox2 interneurons. Bilateral injections of AAV9-CamKII0.4-eGFP into the LPGi in adult *Shox2::Cre*; *Ai9(RCL-tdT)* mice (Figure 2A) labeled LPGi, but labeling also spread beyond these nuclei in the ventral medulla to other neighboring reticulospinal nuclei including the Gi and GiV. We examined resulting projections and terminations in lumbar spinal cord sections (Figure 2B). The distribution of eGFP in the spinal cord matches previous studies examining activation patterns following LPGi stimulation,[33] with hot spots of descending fibers within the lateral white matter columns and dense terminations medially in spinal gray matter. These findings also match what has been shown in anatomical tracing studies of the reticulospinal tract, originating from the LPGi, in adult mice.[39]

The LPGi consists of serotonergic, glutamatergic, GABAergic, and glycinergic neurons.[18,33,40,41] However, the activation of excitatory LPGi neurons, and not glycinergic or GABAergic neurons, was shown to promote forward locomotion in adult mice.[18] We therefore, sought to calculate the proportion of transfected LPGi neurons, which are excitatory. We probed for eGFP RNA to visualize transfected neurons, and VGLUT2 RNA to visualize excitatory neurons (Figure 3A). We found that an average of 42% eGFP RNA$^+$ LPGi neurons were VGLUT2 RNA$^+$ across four mice (Figures 3B and 3C). This suggested that a proportion of excitatory neurons were targeted by our injections into the LPGi. To examine the terminations of the excitatory reticulospinal neurons onto lumbar spinal Shox2 interneurons, we performed immunohistochemistry on spinal cord slices to label VGLUT2$^+$/eGFP$^+$ puncta in apposition to Shox2 interneurons (Figure 3D). We show that, while a subset of lumbar Shox2 interneurons had no VGLUT2$^+$/eGFP$^+$ puncta (Figure 3E), most Shox2 interneurons were 50–200 μm^2 in area and overlapped with 10 or less VGLUT2$^+$/eGFP$^+$ puncta (Figure 3F). Some Shox2 interneurons were considerably larger (300–750 μm^2) and contained higher amounts of overlapping VGLUT2$^+$/eGFP$^+$ puncta (Figure 3F), supporting the notion that lumbar spinal Shox2 interneurons are a heterogeneous population. Moreover, almost half of the eGFP$^+$ puncta on lumbar spinal Shox2 interneurons were VGLUT2$^+$ (Figure 3G). These anatomical data support that Shox2 interneurons receive input from neurons in the caudal ventral medulla, with a subset of it being from excitatory neurons.

Electrophysiology demonstrates a monosynaptic connection between excitatory reticulospinal neurons and lumbar spinal Shox2 interneurons

In order to evaluate the functionality of the connection between excitatory reticulospinal neurons and Shox2 interneurons in the adult mouse, we sought to directly measure the electrophysiological input that Shox2 interneurons receive via these synaptic contacts. To determine the extent to which the observed putative excitatory puncta were functional synapses, we performed bilateral injections of AAV9-CaMKIIa-hChR2(H134R)-EYFP into the LPGi in adult *Shox2::Cre*; *Ai9(RCL-tdT)* mice (Figure 4A). We optically stimulated terminals in the lumbar spinal slice during whole-cell patch clamp

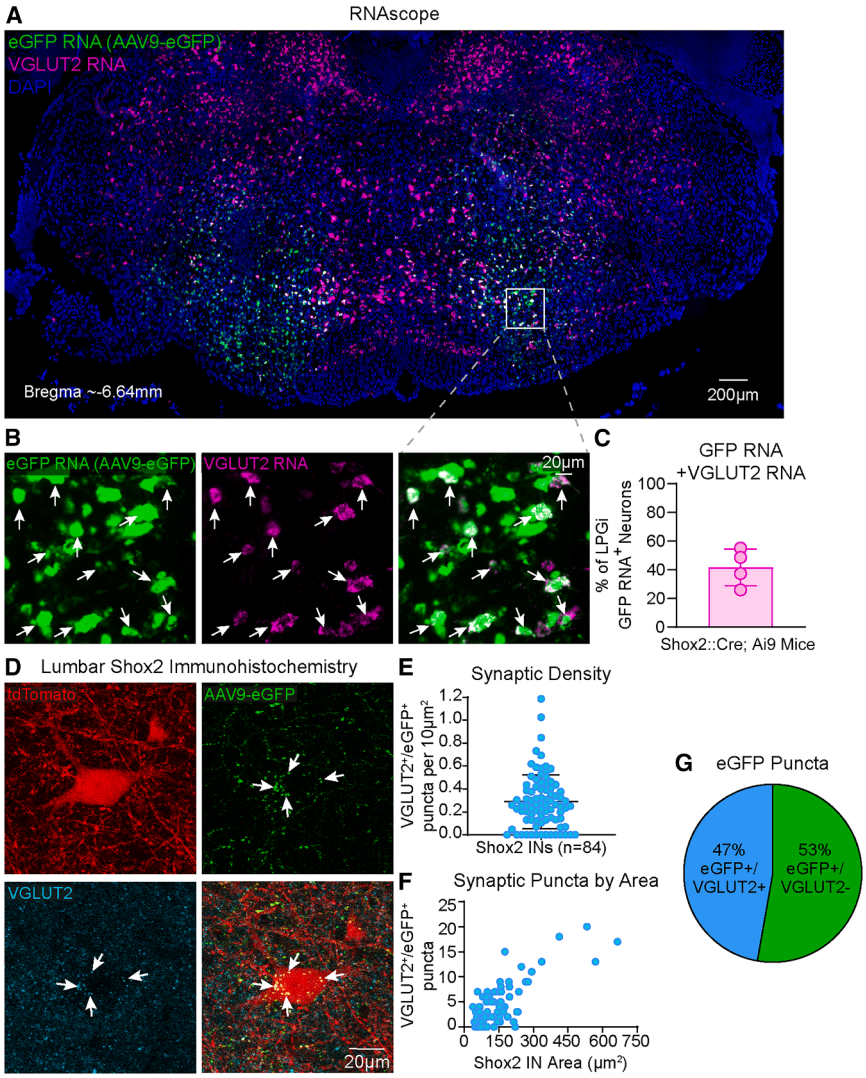

Figure 3. RNAscope in LPGi and immunohistochemistry in lumbar spinal cord reveal excitatory anatomy

(A) RNAscope showing bilateral AAV9-CamKII0.4-eGFP injection (green) and glutamatergic cells signified by VGLUT2 RNA (magenta) with DAPI for whole-slice morphology of brainstem slice (blue) at approximately Bregma −6.64.[38] Scale bars, 200 μm.

(B) Inset of eGFP RNA (green), VGLUT2 RNA (magenta), and overlapping image showing putatively excitatory LPGi neurons. Scale bars, 20 μm.

(C) Approximately 40% of injected, eGFP RNA$^+$, LPGi neurons also are VGLUT2 RNA$^+$.

(D) Immunostaining of lumbar spinal slices from AAV9-eGFP injected mice for VGLUT2 (cyan) shows overlap with eGFP$^+$ terminations (green) onto Shox2 interneurons (red) in confocal images. Scale bars, 20 μm.

(E) The density of putative glutamatergic synaptic contacts from reticulospinal neurons onto lumbar spinal Shox2 interneurons (INs).

(F) Number of putative glutamatergic synaptic contacts plotted against Shox2 interneuron (IN) cross-sectional area.

(G) Of all eGFP+ puncta counted on Shox2 interneurons, 47% were also VGLUT2$^+$. n = 84 lumbar Shox2 interneurons, N = 4 mice.

from visually identified Shox2 interneurons. We did this in both baseline recordings and in the presence of TTX+4-AP to isolate the monosynaptic component of the light-evoked response (Figure 4B). We found that one-third (n = 12/36) of tested Shox2 interneurons displayed baseline light-evoked excitatory postsynaptic currents (EPSCs, Figure 4C). Of this subset, we lost three Shox2 interneurons and were therefore unable to confirm whether the input they received was monosynaptic or polysynaptic. Following TTX+4-AP application, we determined that a subset of Shox2 interneurons received monosynaptic light-evoked input (n = 4/9, Figure 4F). There was no significant change in EPSC amplitude (16.7 ± 6.7 pA) or latency (6.5 ± 1.5 ms) in Shox2 interneurons with detectable inputs remaining, compared to baseline amplitude (25.0 ± 8.8 pA; Figure 4G) and latency (4.9 ± 0.7 ms; Figure 4H). The mean amplitude of the putative-polysynaptic EPSCs recorded in 5 Shox2 interneurons at baseline (23.8 ± 7.8 pA, Figure 4D) was similar to the mean confirmed-monosynaptic EPSC amplitude at baseline (25.0 ± 8.8 pA, Figure 4G). The mean amplitude of the unconfirmed-polysynaptic Shox2 interneurons was 37.1 ± 3.3 pA (Figure 4D). The mean latency of the putative-polysynaptic input to Shox2 interneurons (6.0 ± 1.9 ms, Figure 4E) was also similar to the mean baseline confirmed-monosynaptic EPSC latency (4.9 ± 0.7 ms, Figure 4H) and unconfirmed-polysynaptic Shox2 interneuron mean latency (5.8 ± 1.9 ms, Figure 4E). Taken together, these findings demonstrate that a subset of lumbar spinal Shox2 interneurons receive monosynaptic excitatory input from reticulospinal neurons.

DISCUSSION

We demonstrated that a subset of Shox2 interneurons receive monosynaptic excitatory input from the LPGi in the adult mouse. This study supports that Shox2 interneurons may be an entry point for supraspinal descending drive into spinal locomotor circuitry.

Technical considerations of viral tracing and electrophysiological connectivity testing

We first sought to examine the monosynaptic component of the connection between the LPGi and Shox2 interneurons to corroborate predictions of locomotor-related brainstem centers sending descending drive directly to rhythm-related spinal interneurons.[13,16,17] We chose the CVS-N2c(ΔG) rabies virus-mediated strategy, which has been previously used in mice to examine

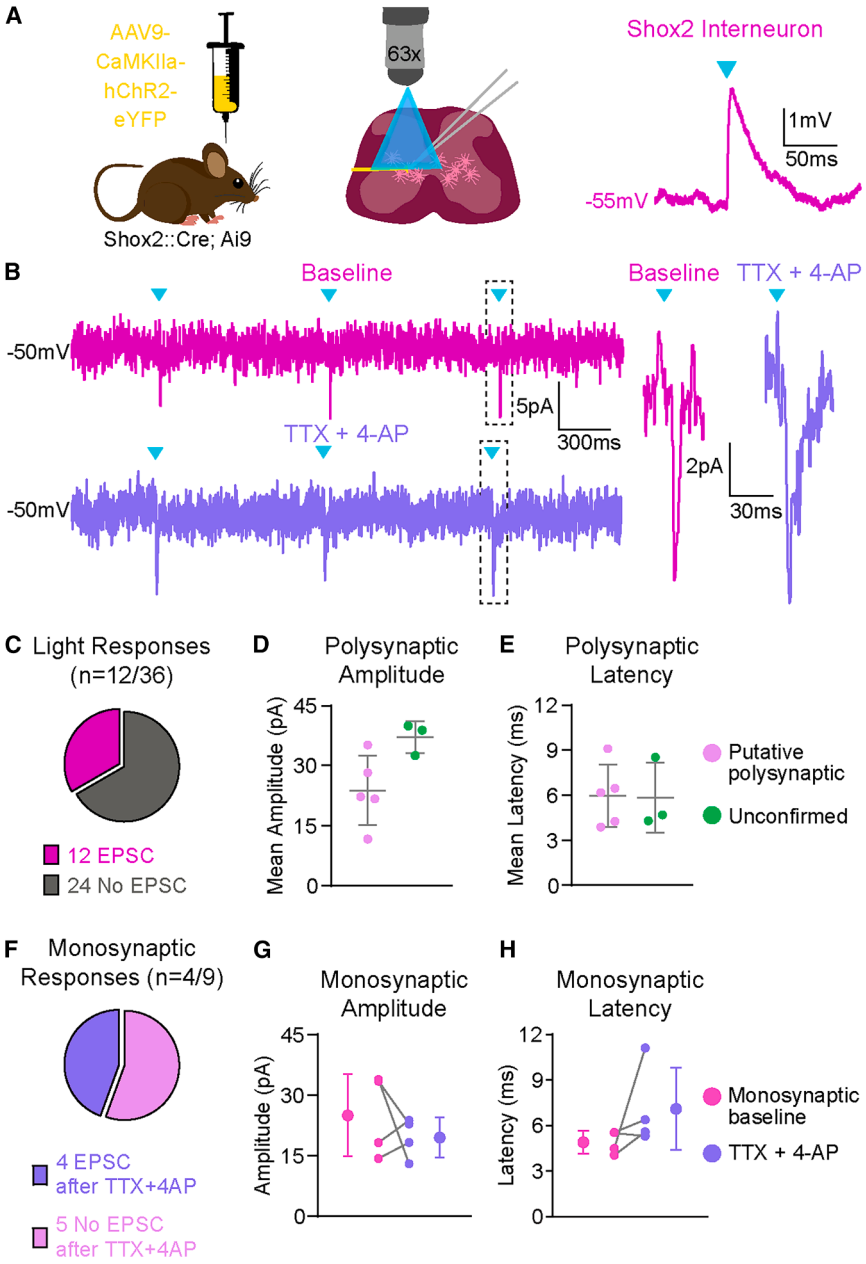

Figure 4. Whole-cell patch clamp recordings of light-evoked reticulospinal terminal activation in Shox2 interneurons

(A) Bilateral injections of AAV9-CaMKIIa-hChR2-eYFP were delivered to adult *Shox2::Cre*; *Ai9(RCL-tdT)* mice. Through the microscope objective, fluorescent light evoked activation of ChR2 in terminals in the lumbar spinal slice during whole-cell patch clamp of Shox2 interneurons. In current-clamp mode, light evoked excitatory postsynaptic potentials. Scale bars, 1 mV, 50 ms.

(B) Light pulse trains evoked excitatory postsynaptic currents in Shox2 interneurons in baseline ACSF (magenta), which had a monosynaptic component revealed after the bath application of TTX + 4-AP (purple). Left scale bars, 5 pA, 300 ms. Inset scale bars, 2 pA, 30 ms.

(C) Of the 36 Shox2 interneurons recorded from, 12 displayed light-evoked excitatory postsynaptic potentials in baseline ACSF conditions. Three of the 12 interneurons with responses were lost after baseline recordings.

(D) Amplitude and (E) latency of 3 unconfirmed-polysynaptic (green) and 5 putative-polysynaptic (pink) Shox2 interneurons.

(F) Of the 9 Shox2 interneurons with light-evoked EPSCs that were tested further, 4 had light-evoked EPSCs, which persisted following bath application of TTX + 4-AP.

(G and H) Amplitude (G) and latency (H) of 4 monosynaptic Shox2 interneurons in baseline (purple) and drug (magenta) conditions. *N* = 7 mice.

monosynaptic inputs to V1 interneurons.[29] The use of the CVS-N2c(ΔG) rabies virus has advantages over earlier strains in that it allows efficient and intense labeling of neuronal somas and processes over long distances in a G protein-dependent/monosynaptic-restricted fashion.[37,42,43] However, it is impossible to determine the true number of starter neurons due to the toxicity of the CVS-N2c(ΔG) rabies virus, although less toxic than other strains.[37] Further, the starter population is likely to be an underestimation or a small subset of the local Shox2 interneuron population due to the necessity of three essential components (TVA, G, and N2c[ΔG]) to be successfully expressed in the same neuron. Nevertheless, we were able to identify labeled spinal starter neurons and synaptically coupled neurons in the spinal cord and brainstem.

Anterograde AAV tracing was used to complement the retrograde tracing and to examine the termination pattern of the LPGi reticulospinal neurons in the lumbar spinal cords of adult mice. Due to the extent and irregular borders of the LPGi, there was spread of labeling to the neighboring structures in the caudal medulla, specifically Gi and GiV. However, our findings are comparable to what has been previously described in the neonatal *in vitro* preparation[33] and in the adult mouse using biotinylated dextran amine solution.[39] We chose the CaMKIIα promoter for its specificity to supraspinal excitatory neurons.[44] More recently however, it has been shown that viral labeling using a CaMKIIα promoter is efficient in both excitatory and inhibitory supraspinal neurons.[45] Our findings support this, as we demonstrate that only about half of the targeted cells in the LPGi labeled in our anterograde AAV tracing experiments are VGLUT2 RNA$^+$. The LPGi includes serotonergic, glutamatergic, GABAergic, and glycinergic neurons.[18,33,40,41] None of these discrete neuronal types in the LPGi have identified spinal targets beyond the excitatory connections to Shox2 interneurons presented in this study. Moreover, it is likely that LPGi inputs to different subsets of Shox2 and other spinal interneurons are serotonergic, excitatory, and inhibitory.

Only excitatory light-evoked responses from reticulospinal neurons in the spinal slice were recorded in this study. Electrophysiological testing may underestimate the connections between the targeted descending neurons and Shox2 interneurons for many reasons. We may be eliminating some of the synaptic connections onto Shox2 interneurons during slice collection due to the removal of dendritic arbors, which extend away from the Shox2 interneuron soma beyond the range of each 300 μm slice. We are also unable to determine how many synaptic contacts are necessary for the light-evoked EPSCs. The amplitude of the light-evoked EPSCs is also likely dictated by light intensity, and ours was relatively low compared to similar experiments.[29] We confirmed that a subset of the light-evoked responses were monosynaptic using pharmacology. The expected response latency at room temperature is unknown but we did expect to see a distinction between confirmed-monosynaptic and at least a portion of the responses that were abolished in TTX+4-AP. It is possible that the quality of the recording was reduced with time.

Adult lumbar Shox2 interneurons likely integrate information broadly from reticular and local spinal sources

Experiments aimed at determining the function of genetically identified locomotor circuit interneurons have largely been carried out in neonatal animals,[26,31,46] with some exceptions.[27,47,48] This is particularly true of rhythm-generating populations, since most of the manipulations affect respiratory function and/or feeding, limiting viability.[3,6,7] This is in contrast with the majority of experiments that determined the roles of various reticulospinal populations. These were largely performed in adult mice, due to the use of viral tools, which require weeks to express.[18–20,47,49,50] The direct excitatory connections demonstrated in this study are likely present at birth, as reticulospinal input develops embryonically.[51] Further, descending fiber-evoked locomotion is reduced in frequency when Shox2 neurons are synaptically silenced[3] and stimulation of the LPGi induces locomotor-like activity[33] in the reduced neonatal mouse preparation. Thus, it is possible that prior demonstrations of reticulospinal activation evoking locomotor-like activity in neonatal preparations[11,33] are via this pathway.

Although the identities of the spinal neurons presynaptic to Shox2 interneurons were not explored, the locations of the presynaptic neurons offer hints to the spinal circuit architecture. Local presynaptic neurons were found in most laminae but there were concentrations in the deep dorsal horn and in the medial ventral horn (lamina VIII). Commissural interneurons are concentrated in lamina VIII.[52,53] At least a subset of Shox2 interneurons activate commissural interneurons[3] but the connection between commissural neurons and Shox2 (or rhythm generating) interneurons is predicted to be important for the coordination of left and right sides during locomotion.[54] Deep dorsal presynaptic neurons would be consistent with those in reflex pathways to rhythm generating neurons,[55,56] which have been shown to be both excitatory and inhibitory to Shox2 interneurons in both neonate[57] and adult.[58] Other local neurons in lamina VII are also expected to be connected, including other Shox2 neurons[10] in addition to V1 and V2b inhibitory interneurons involved in flexor-extensor alternation.[30,59,60] The direct testing of the connectivity of these populations is complicated by the downregulation of the expression of the identifying transcription factors. It is clear that Shox2 interneurons broadly receive input from spinal neurons, which may be integrated into their rhythmogenic output in locomotor circuitry.

Potential behavioral implications including the initiation of forward locomotion

In the mammalian medullary reticular formation, regional borders are ambiguous and neuronal cell types are diverse.[61] Robust behavioral effects after the manipulation of specific medullary neuronal populations have been evoked in many motor-related contexts in mice, including ipsilateral body turning,[20] locomotor arrest,[19] REM sleep, and associated muscle atonia,[62] and even wakefulness with strong postural tone from coma.[63] Based on the monosynaptically connected medullary nuclei identified in this study, Shox2 interneurons may play a role in these and other motor functions. It is possible that subsets of lumbar spinal Shox2 interneurons play regulatory roles in posture and gait, as suggested by their direct input from vestibular nuclei such as the lateral vestibular nucleus.[64] Shox2 interneurons may also directly integrate raphespinal input in the context of locomotion, as the caudal raphe nuclei, including the raphe pallidus have been implicated in forward locomotion.[65] The nature and utility of these connections to lumbar spinal Shox2 interneurons are likely varied and relevant to broad arrays of behavioral outcomes.

The LPGi alone is implicated in muscle atonia and postural control in addition to locomotion, with the neurons controlling these behaviors likely intermingled within this region.[66] Other functions the LPGi has been implicated include sexual reflexes in male rodents,[67,68] audition,[69] pain,[40] bladder control,[41] and cardiac function.[70] Previous studies have also demonstrated the role of the LPGi in general arousal.[71–73] This is likely via the dense connections from the LPGi to the locus coeruleus, which are comprised of excitatory and inhibitory projection neurons and have been shown to collateralize to innervate the spinal cord as well.[72] It is unclear how many simultaneously ascending and descending neurons exist in reticular nuclei, let alone the LPGi.[74] Lumbar spinal Shox2 interneurons may integrate excitatory and inhibitory input from descending bifurcating neurons to modulate features of locomotor behavior.

Direct unilateral activation of excitatory LPGi neurons results in the initiation of locomotion, which can be driven in a speed-dependent manner,[18] and has been reproduced using computational modeling.[16] As putative rhythm-generating neurons of the central pattern generator and direct recipients of excitatory reticulospinal input from the LPGi, spinal Shox2 interneurons are poised to mediate these effects. The identities and locations of the excitatory LPGi neurons necessary for the initiation of locomotion, and what proportion of these are present in this study as monosynaptic partners to Shox2 interneurons is unknown. Future investigations are also needed to delineate the utility of the connection between the LPGi and lumbar spinal Shox2 interneurons in the context of motor and other behaviors, including and beyond the excitatory connections identified in this study.

Limitations of the study

This study primarily focused on identifying a monosynaptic connection between the LPGi in the medulla and lumbar spinal Shox2 interneurons in adult mouse. First, this study was limited

by the toxicity[37] and efficacy of the viruses used for anatomical tracing. The CVS-N2c(ΔG) rabies virus-mediated strategy is toxic to neurons, although less toxic than alternative strategies.[37] This strategy also required a combination of factors to be expressed in the same starter Shox2 interneurons, limiting the efficacy. Second, the stimulation of the LPGi neuron somatas, rather than optogenetic stimulation of terminals in spinal slice, would be more physiologically relevant. However, such a manipulation is unfeasible in the adult mouse *in vitro*, as the isolated brainstem-spinal cord preparation would be inviable, and also *in vivo*, as the recordings cannot be made from visually identified neurons. Finally, manipulations in this study were limited by the ambiguous anatomical borders within the ventral medulla. The LPGi was targeted during viral injections purely using co-ordinates from Bregma.[38] In the future, perhaps a more advanced understanding of the discrete neuronal populations in the LPGi will lead to more precise targeting.

RESOURCE AVAILABILITY

Lead contact

Requests for further information should be directed to Kimberly J. Dougherty (kjd86@drexel.edu).

Materials availability

This study did not generate new reagents.

Data and code availability

- All data generated in this study are available in the article.
- The original MATLAB code used in this work is available online (https://github.com/heyshayna/SinghBrainstemManuscript2025).
- Any additional information required to reanalyze the data reported in this paper is available upon request.

ACKNOWLEDGMENTS

We thank members of the Marion Murray Spinal Cord Research Center and Drexel University Lab Animal Resources for support. We thank Rémi Ronzano, Mary Patton, Anand Kulkarni, and Jay Bikoff for experimental advice. We thank Julien Bouyer, Ying Jin, Wenqiang Huang, and Dong Wang for generous surgical assistance. We also thank Lynnette Montgomery for discussions and Malcolm Jennings for experimental assistance. This work was supported by NIH R01 NS130799 (K.J.D.), T32 NS121768 (S.S.), and F31 NS132514 (S.S.). Modified rabies virus was provided by the NIH Virus Center supported by P40 OD010996.

AUTHOR CONTRIBUTIONS

S.S. and K.J.D. conceptualized the study. S.S. performed surgical procedures and electrophysiology experiments. S.S. and L.Y. performed histology experiments. S.S. and K.J.D. analyzed the data. S.S. and K.J.D. wrote the manuscript with input from L.Y.

DECLARATION OF INTERESTS

The authors declare no competing interests.

STAR★METHODS

Detailed methods are provided in the online version of this paper and include the following:

SUPPLEMENTAL INFORMATION

Supplemental information can be found online at https://doi.org/10.1016/j.isci.2025.114567.

Received: August 1, 2025
Revised: October 28, 2025
Accepted: December 23, 2025
Published: December 29, 2025

REFERENCES

1. Dougherty, K.J. (2023). Distinguishing subtypes of spinal locomotor neurons to inform circuit function and dysfunction. Curr. Opin. Neurobiol. *82*, 102763. https://doi.org/10.1016/j.conb.2023.102763.
2. Brownstone, R.M., and Bui, T.V. (2010). Spinal interneurons providing input to the final common path during locomotion. Prog. Brain Res. *187*, 81–95. https://doi.org/10.1016/B978-0-444-53613-6.00006-X.
3. Dougherty, K.J., Zagoraiou, L., Satoh, D., Rozani, I., Doobar, S., Arber, S., Jessell, T.M., and Kiehn, O. (2013). Locomotor Rhythm Generation Linked to the Output of Spinal Shox2 Excitatory Interneurons. Neuron *80*, 920–933. https://doi.org/10.1016/j.neuron.2013.08.015.
4. Brownstone, R.M., and Wilson, J.M. (2008). Strategies for delineating spinal locomotor rhythm-generating networks and the possible role of Hb9 interneurones in rhythmogenesis. Brain Res. Rev. *57*, 64–76. https://doi.org/10.1016/j.brainresrev.2007.06.025.
5. Hinckley, C.A., and Ziskind-Conhaim, L. (2006). Electrical coupling between locomotor-related excitatory interneurons in the mammalian spinal cord. J. Neurosci. *26*, 8477–8483. https://doi.org/10.1523/JNEUROSCI.0395-06.2006.
6. Caldeira, V., Dougherty, K.J., Borgius, L., and Kiehn, O. (2017). Spinal Hb9::Cre-derived excitatory interneurons contribute to rhythm generation in the mouse. Sci. Rep. *7*, 41369. https://doi.org/10.1038/srep41369.
7. Bertho, M., Caldeira, V., Hsu, L.J., Löw, P., Borgius, L., and Kiehn, O. (2024). Excitatory Spinal Lhx9-Derived Interneurons Modulate Locomotor Frequency in Mice. J. Neurosci. *44*, e1607232024. https://doi.org/10.1523/JNEUROSCI.1607-23.2024.
8. Chalif, J.I., Martínez-Silva, M.d.L., Pagiazitis, J.G., Murray, A.J., and Mentis, G.Z. (2022). Control of mammalian locomotion by ventral spinocerebellar tract neurons. Cell *185*, 328–344.e26. https://doi.org/10.1016/j.cell.2021.12.014.
9. Singh, S., Shevtsova, N.A., Yao, L., Rybak, I.A., and Dougherty, K.J. (2025). Properties of rhythmogenic currents in spinal Shox2 interneurons across postnatal development. J. Physiol. *603*, 3201–3221. https://doi.org/10.1113/JP287752.
10. Ha, N.T., and Dougherty, K.J. (2018). Spinal Shox2 interneuron interconnectivity related to function and development. eLife *7*, e42519. https://doi.org/10.7554/eLife.42519.001.
11. Hägglund, M., Borgius, L., Dougherty, K.J., and Kiehn, O. (2010). Activation of groups of excitatory neurons in the mammalian spinal cord or hindbrain evokes locomotion. Nat. Neurosci. *13*, 246–252. https://doi.org/10.1038/nn.2482.
12. Noga, B.R., Kettler, J., and Jordan, L.M. (1988). Locomotion Produced in Mesencephalic Cats by Injections of Putative Transmitter Substances and Antagonists into the Medial Reticular Formation and the Pontomedullary Locomotor Strip. J. Neurosci. *8*, 2074–2086.
13. Noga, B.R., Kriellaars, D.J., Brownstone, R.M., and Jordan, L.M. (2003). Mechanism for activation of locomotor centers in the spinal cord by

stimulation of the mesencephalic locomotor region. J. Neurophysiol. *90*, 1464–1478. https://doi.org/10.1152/jn.00034.2003.

14. Opris, I., Dai, X., Johnson, D.M.G., Sanchez, F.J., Villamil, L.M., Xie, S., Lee-Hauser, C.R., Chang, S., Jordan, L.M., and Noga, B.R. (2019). Activation of Brainstem Neurons During Mesencephalic Locomotor Region-Evoked Locomotion in the Cat. Front. Syst. Neurosci. *13*, 69. https://doi.org/10.3389/fnsys.2019.00069.
15. Lloyd, D.P.C. (1941). Activity in neurons of the bulbospinal correlation system. J. Neurophysiol. *4*, 115–134. https://doi.org/10.1152/jn.1941.4.1.115.
16. Ausborn, J., Shevtsova, N.A., Caggiano, V., Danner, S.M., and Rybak, I.A. (2019). Computational modeling of brainstem circuits controlling locomotor frequency and gait. eLife *8*, e43587. https://doi.org/10.7554/eLife.43587.001.
17. Kim, L.H., Sharma, S., Sharples, S.A., Mayr, K.A., Kwok, C.H.T., and Whelan, P.J. (2017). Integration of descending command systems for the generation of context-specific locomotor behaviors. Front. Neurosci. *11*, 581. https://doi.org/10.3389/fnins.2017.00581.
18. Capelli, P., Pivetta, C., Soledad Esposito, M., and Arber, S. (2017). Locomotor speed control circuits in the caudal brainstem. Nature *551*, 373–377. https://doi.org/10.1038/nature24064.
19. Bouvier, J., Caggiano, V., Leiras, R., Caldeira, V., Bellardita, C., Balueva, K., Fuchs, A., and Kiehn, O. (2015). Descending Command Neurons in the Brainstem that Halt Locomotion. Cell *163*, 1191–1203. https://doi.org/10.1016/j.cell.2015.10.074.
20. Cregg, J.M., Leiras, R., Montalant, A., Wanken, P., Wickersham, I.R., and Kiehn, O. (2020). Brainstem neurons that command mammalian locomotor asymmetries. Nat. Neurosci. *23*, 730–740. https://doi.org/10.1038/s41593-020-0633-7.
21. Bannatyne, B.A., Edgley, S.A., Hammar, I., Jankowska, E., and Maxwell, D.J. (2003). Networks of inhibitory and excitatory commissural interneurons mediating crossed reticulospinal actions. Eur. J. Neurosci. *18*, 2273–2284. https://doi.org/10.1046/j.1460-9568.2003.02973.x.
22. Szokol, K., Glover, J.C., and Perreault, M.-C. (2011). Organization of functional synaptic connections between medullary reticulospinal neurons and lumbar descending commissural interneurons in the neonatal mouse. J. Neurosci. *31*, 4731–4742. https://doi.org/10.1523/JNEUROSCI.5486-10.2011.
23. Matsuyama, K., Nakajima, K., Mori, F., Aoki, M., and Mori, S. (2004). Lumbar commissural interneurons with reticulospinal inputs in the cat: Morphology and discharge patterns during fictive locomotion. J. Comp. Neurol. *474*, 546–561. https://doi.org/10.1002/cne.20131.
24. Ohta, Y., and Grillner, S. (1989). Monosynaptic Excitatory Amino Acid Transmission From the Posterior Rhombencephalic Reticular Nucleus to Spinal Neurons Involved in the Control of Locomotion in Lamprey. J Neurophysiol. *62*, 1079–1089.
25. Kathe, C., Skinnider, M.A., Hutson, T.H., Regazzi, N., Gautier, M., Demesmaeker, R., Komi, S., Ceto, S., James, N.D., Cho, N., et al. (2022). The neurons that restore walking after paralysis. Nature *611*, 540–547. https://doi.org/10.1038/s41586-022-05385-7.
26. Crone, S.A., Quinlan, K.A., Zagoraiou, L., Droho, S., Restrepo, C.E., Lundfald, L., Endo, T., Setlak, J., Jessell, T.M., Kiehn, O., et al. (2008). Genetic Ablation of V2a Ipsilateral Interneurons Disrupts Left-Right Locomotor Coordination in Mammalian Spinal Cord. Neuron *60*, 70–83. https://doi.org/10.1016/j.neuron.2008.08.009.
27. Crone, S.A., Zhong, G., Harris-Warrick, R., and Sharma, K. (2009). In mice lacking V2a interneurons, gait depends on speed of locomotion. J. Neurosci. *29*, 7098–7109. https://doi.org/10.1523/JNEUROSCI.1206-09.2009.
28. Vieillard, J., Franck, M.C.M., Hartung, S., Jakobsson, J.E.T., Ceder, M.M., Welsh, R.E., Lagerström, M.C., and Kullander, K. (2023). Adult spinal Dmrt3 neurons receive direct somatosensory inputs from ipsi- and contralateral primary afferents and from brainstem motor nuclei. J. Comp. Neurol. *531*, 5–24. https://doi.org/10.1002/cne.25405.
29. Chapman, P.D., Kulkarni, A.S., Trevisan, A.J., Han, K., Hinton, J.M., Deltuvaite, P., Fenno, L.E., Ramakrishnan, C., Patton, M.H., Schwarz, L.A., et al. (2025). A brain-wide map of descending inputs onto spinal V1 interneurons. Neuron *113*, 524–538.e6. https://doi.org/10.1016/j.neuron.2024.11.019.
30. Britz, O., Zhang, J., Grossmann, K.S., Dyck, J., Kim, J.C., Dymecki, S., Gosgnach, S., and Goulding, M. (2015). A genetically defined asymmetry underlies the inhibitory control of flexor–extensor locomotor movements. eLife *4*, e04718. https://doi.org/10.7554/eLife.04718.
31. Gosgnach, S., Lanuza, G.M., Butt, S.J.B., Saueressig, H., Zhang, Y., Velasquez, T., Riethmacher, D., Callaway, E.M., Kiehn, O., and Goulding, M. (2006). V1 spinal neurons regulate the speed of vertebrate locomotor outputs. Nature *440*, 215–219. https://doi.org/10.1038/nature04545.
32. Petras, J.M. (1967). Cortical, tectal and tegmental fiber connections in the spinal cord of the cat. Brain Res. *6*, 275–324. https://doi.org/10.1016/0006-8993(67)90196-5.
33. Hsu, L.J., Bertho, M., and Kiehn, O. (2023). Deconstructing the modular organization and real-time dynamics of mammalian spinal locomotor networks. Nat. Commun. *14*, 873. https://doi.org/10.1038/s41467-023-36587-w.
34. Baker, S.N., and Perez, M.A. (2017). Reticulospinal contributions to gross hand function after human spinal cord injury. J. Neurosci. *37*, 9778–9784. https://doi.org/10.1523/JNEUROSCI.3368-16.2017.
35. May, Z., Fenrich, K.K., Dahlby, J., Batty, N.J., Torres-Espín, A., and Fouad, K. (2017). Following Spinal Cord Injury Transected Reticulospinal Tract Axons Develop New Collateral Inputs to Spinal Interneurons in Parallel with Locomotor Recovery. Neural Plast. *2017*, 1932875. https://doi.org/10.1155/2017/1932875.
36. Asboth, L., Friedli, L., Beauparlant, J., Martinez-Gonzalez, C., Anil, S., Rey, E., Baud, L., Pidpruzhnykova, G., Anderson, M.A., Shkorbatova, P., et al. (2018). Cortico–reticulo–spinal circuit reorganization enables functional recovery after severe spinal cord contusion. Nat. Neurosci. *21*, 576–588. https://doi.org/10.1038/s41593-018-0093-5.
37. Reardon, T.R., Murray, A.J., Turi, G.F., Wirblich, C., Croce, K.R., Schnell, M.J., Jessell, T.M., and Losonczy, A. (2016). Rabies Virus CVS-N2c ΔG Strain Enhances Retrograde Synaptic Transfer and Neuronal Viability. Neuron *89*, 711–724. https://doi.org/10.1016/j.neuron.2016.01.004.
38. Paxinos, G., and Franklin, K.B.J. (2004). The Mouse Brain in Stereotaxic Coordinates, 2nd ed. (Academic Press).
39. Liang, H., Watson, C., and Paxinos, G. (2016). Terminations of reticulospinal fibers originating from the gigantocellular reticular formation in the mouse spinal cord. Brain Struct. Funct. *221*, 1623–1633. https://doi.org/10.1007/s00429-015-0993-z.
40. Ganley, R.P., de Sousa, M.M., Werder, K., Öztürk, T., Mendes, R., Ranucci, M., Wildner, H., and Zeilhofer, H.U. (2023). Targeted anatomical and functional identification of antinociceptive and pronociceptive serotonergic neurons that project to the spinal dorsal horn. eLife *12*, e78689. https://doi.org/10.7554/eLife.78689.
41. Talluri, B., Hoelzel, F., Medda, B.K., Terashvili, M., Sanvanson, P., Shaker, R., Banerjee, A., Sengupta, J.N., and Banerjee, B. (2022). Identification and characterization of rostral ventromedial medulla neurons synaptically connected to the urinary bladder afferents in female rats with or without neonatal cystitis. J. Comp. Neurol. *530*, 1129–1147. https://doi.org/10.1002/cne.25260.
42. Wickersham, I.R., Finke, S., Conzelmann, K.-K., and Callaway, E.M. (2007). Retrograde neuronal tracing with a deletion-mutant rabies virus. Nat. Methods *4*, 47–49. https://doi.org/10.1038/nmeth999.
43. Wickersham, I.R., Lyon, D.C., Barnard, R.J.O., Mori, T., Finke, S., Conzelmann, K.-K., Young, J.A.T., and Callaway, E.M. (2007). Monosynaptic Restriction of Transsynaptic Tracing from Single, Genetically Targeted Neurons. Neuron *53*, 639–647. https://doi.org/10.1016/j.neuron.2007.01.033.
44. Yizhar, O., Fenno, L.E., Davidson, T.J., Mogri, M., and Deisseroth, K. (2011). Optogenetics in Neural Systems. Neuron *71*, 9–34. https://doi.org/10.1016/j.neuron.2011.06.004.

45. Veres, J.M., Andrasi, T., Nagy-Pal, P., and Hajos, N. (2023). CaMKIIα Promoter-Controlled Circuit Manipulations Target Both Pyramidal Cells and Inhibitory Interneurons in Cortical Networks. eNeuro *10*, ENEURO.0070-23.2023. https://doi.org/10.1523/ENEURO.0070-23.2023.

46. Lanuza, G.M., Gosgnach, S., Pierani, A., Jessell, T.M., and Goulding, M. (2004). Genetic Identification of Spinal Interneurons that Coordinate Left-Right Locomotor Activity Necessary for Walking Movements. Neuron *42*, 375–386. https://doi.org/10.1016/S0896-6273(04)00249-1.

47. Talpalar, A.E., Bouvier, J., Borgius, L., Fortin, G., Pierani, A., and Kiehn, O. (2013). Dual-mode operation of neuronal networks involved in left-right alternation. Nature *500*, 85–88. https://doi.org/10.1038/nature12286.

48. Koronfel, L.M., Kanning, K.C., Alcos, A., Henderson, C.E., and Brownstone, R.M. (2021). Elimination of glutamatergic transmission from Hb9 interneurons does not impact treadmill locomotion. Sci. Rep. *11*, 16008. https://doi.org/10.1038/s41598-021-95143-y.

49. Esposito, M.S., Capelli, P., and Arber, S. (2014). Brainstem nucleus MdV mediates skilled forelimb motor tasks. Nature *508*, 351–356. https://doi.org/10.1038/nature13023.

50. Usseglio, G., Gatier, E., Heuzé, A., Hérent, C., and Bouvier, J. (2020). Control of Orienting Movements and Locomotion by Projection-Defined Subsets of Brainstem V2a Neurons. Curr. Biol. *30*, 4665–4681.e6. https://doi.org/10.1016/j.cub.2020.09.014.

51. Perreault, M.C., and Glover, J.C. (2013). Glutamatergic reticulospinal neurons in the mouse: developmental origins, axon projections, and functional connectivity. Ann. N. Y. Acad. Sci. *1279*, 80–89. https://doi.org/10.1111/nyas.12054.

52. Eide, A.-L., Glover, J., Kjaerulff, O., and Kiehn, O. (1999). Characterization of commissural interneurons in the lumbar region of the neonatal rat spinal cord. J. Comp. Neurol. *403*, 332–345.

53. Jankowska, E., and Noga, B.R. (1990). Contralaterally projecting lamina VIII interneurones in middle lumbar segments in the cat. Brain Res. *535*, 327–330. https://doi.org/10.1016/0006-8993(90)91618-Q.

54. Shevtsova, N.A., Talpalar, A.E., Markin, S.N., Harris-Warrick, R.M., Kiehn, O., and Rybak, I.A. (2015). Organization of left–right coordination of neuronal activity in the mammalian spinal cord: Insights from computational modelling. J. Physiol. *593*, 2403–2426. https://doi.org/10.1113/JP270121.

55. Domínguez-Rodríguez, L.E., Stecina, K., García-Ramírez, D.L., Mena-Avila, E., Milla-Cruz, J.J., Martínez-Silva, L., Zhang, M., Hultborn, H., and Quevedo, J.N. (2020). Candidate Interneurons Mediating the Resetting of the Locomotor Rhythm by Extensor Group I Afferents in the Cat. Neuroscience *450*, 96–112. https://doi.org/10.1016/j.neuroscience.2020.09.017.

56. Frigon, A., Akay, T., and Prilutsky, B.I. (2022). Control of Mammalian Locomotion by Somatosensory Feedback. Compr. Physiol. *12*, 2877–2947. https://doi.org/10.1002/j.2040-4603.2022.tb00203.x.

57. Li, E.Z., Garcia-Ramirez, D.L., and Dougherty, K.J. (2019). Flexor and Extensor Ankle Afferents Broadly Innervate Locomotor Spinal Shox2 Neurons and Induce Similar Effects in Neonatal Mice. Front. Cell. Neurosci. *13*, 452. https://doi.org/10.3389/fncel.2019.00452.

58. Garcia-Ramirez, D.L., Ha, N.T., Bibu, S., Stachowski, N.J., and Dougherty, K.J. (2021). Spinal cord injury alters spinal Shox2 interneurons by enhancing excitatory synaptic input and serotonergic modulation while maintaining intrinsic properties in mouse. J. Neurosci. *41*, 5833–5848. https://doi.org/10.1523/JNEUROSCI.1576-20.2021.

59. Shevtsova, N.A., and Rybak, I.A. (2016). Organization of flexor–extensor interactions in the mammalian spinal cord: insights from computational modelling. J. Physiol. *594*, 6117–6131. https://doi.org/10.1113/JP272437.

60. Shevtsova, N.A., Li, E.Z., Singh, S., Dougherty, K.J., and Rybak, I.A. (2022). Ipsilateral and Contralateral Interactions in Spinal Locomotor Circuits Mediated by V1 Neurons: Insights from Computational Modeling. Int. J. Mol. Sci. *23*, 5541. https://doi.org/10.3390/ijms23105541.

61. Ascenzi, B.M. (2025). The Reticular Formation. In From Anatomy to Function of the Central Nervous System, B.M. Ascenzi, ed. (Elsevier), pp. 163–210. https://doi.org/10.1016/B978-0-12-822404-5.00007-3.

62. Weber, F., Chung, S., Beier, K.T., Xu, M., Luo, L., and Dan, Y. (2015). Control of REM sleep by ventral medulla GABAergic neurons. Nature *526*, 435–438. https://doi.org/10.1038/nature14979.

63. Gao, S., Proekt, A., Renier, N., Calderon, D.P., and Pfaff, D.W. (2019). Activating an anterior nucleus gigantocellularis subpopulation triggers emergence from pharmacologically-induced coma in rodents. Nat. Commun. *10*, 2897. https://doi.org/10.1038/s41467-019-10797-7.

64. Witts, E.C., and Murray, A.J. (2019). Vestibulospinal contributions to mammalian locomotion. Curr. Opin. Physiol. *8*, 56–62. https://doi.org/10.1016/j.cophys.2018.12.010.

65. Jordan, L.M. (1998). Initiation of Locomotion in Mammals. Ann. N. Y. Acad. Sci. *860*, 83–93. https://doi.org/10.1111/j.1749-6632.1998.tb09040.x.

66. Perreault, M.-C., and Giorgi, A. (2019). Diversity of reticulospinal systems in mammals. Curr. Opin. Physiol. *8*, 161–169. https://doi.org/10.1016/j.cophys.2019.03.001.

67. Marson, L., List, M.S., and McKenna, K.E. (1992). Lesions of the nucleus paragigantocellularis alter ex copula penile reflexes. Brain Res. *592*, 187–192. https://doi.org/10.1016/0006-8993(92)91675-5.

68. Liu, Y.-C., and Sachs, B.D. (1999). Erectile function in male rats after lesions in the lateral paragigantocellular nucleus. Neurosci. Lett. *262*, 203–206. https://doi.org/10.1016/S0304-3940(99)00070-1.

69. Bellintani-Guardia, B., Schweizer, M., and Herbert, H. (1996). Analysis of projections from the cochlear nucleus to the lateral paragigantocellular reticular nucleus in the rat. Cell Tissue Res. *283*, 493–505. https://doi.org/10.1007/s004410050560.

70. Dergacheva, O., Wang, X., Lovett-Barr, M.R., Jameson, H., and Mendelowitz, D. (2010). The lateral paragigantocellular nucleus modulates parasympathetic cardiac neurons: A mechanism for rapid eye movement sleep-dependent changes in heart rate. J. Neurophysiol. *104*, 685–694. https://doi.org/10.1152/jn.00228.2010.

71. Zhang, Z., Su, J., Tang, J., Chung, L., Page, J.C., Winter, C.C., Liu, Y., Kegeles, E., Conti, S., Zhang, Y., et al. (2024). Spinal projecting neurons in rostral ventromedial medulla co-regulate motor and sympathetic tone. Cell *187*, 3427–3444.e21. https://doi.org/10.1016/j.cell.2024.04.022.

72. Van Bockstaele, E.J., and Aston-Jones, G. (1995). Integration in the Ventral Medulla and Coordination of Sympathetic, Pain and Arousal Functions. Clin. Exp. Hypertens. *17*, 153–165. https://doi.org/10.3109/10641969509087062.

73. Guyenet, P.G., Darnall, R.A., and Riley, T.A. (1990). Rostral ventrolateral medulla and sympathorespiratory integration in rats. Am. J. Physiol. *259*, R1063–R1074. https://doi.org/10.1152/ajpregu.1990.259.5.R1063.

74. Pfaff, D.W., Martin, E.M., and Faber, D. (2012). Origins of arousal: roles for medullary reticular neurons. Trends Neurosci. *35*, 468–476. https://doi.org/10.1016/j.tins.2012.04.008.

75. Lee, J.H., Durand, R., Gradinaru, V., Zhang, F., Goshen, I., Kim, D.S., Fenno, L.E., Ramakrishnan, C., and Deisseroth, K. (2010). Global and local fMRI signals driven by neurons defined optogenetically by type and wiring. Nature *465*, 788–792. https://doi.org/10.1038/nature09108.

76. Watabe-Uchida, M., Zhu, L., Ogawa, S.K., Vamanrao, A., and Uchida, N. (2012). Whole-brain mapping of direct inputs to midbrain dopamine neurons. Neuron *74*, P858–P873. https://doi.org/10.1016/j.neuron.2012.03.017.

77. Madisen, L., Zwingman, T.A., Sunkin, S.M., Oh, S.W., Zariwala, H.A., Gu, H., Ng, L.L., Palmiter, R.D., Hawrylycz, M.J., Jones, A.R., et al. (2010). A robust and high-throughput Cre reporting and characterization system for the whole mouse brain. Nat. Neurosci. *13*, 133–140. https://doi.org/10.1038/nn.2467.

78. Wang, F., Flanagan, J., Su, N., Wang, L.C., Bui, S., Nielson, A., Wu, X., Vo, H.T., Ma, X.J., and Luo, Y. (2012). RNAscope: A novel *in situ* RNA analysis platform for formalin-fixed, paraffin-embedded tissues. J. Mol. Diagn. *14*, 22–29. https://doi.org/10.1016/j.jmoldx.2011.08.002.

79. Collins, T.J. (2007). ImageJ for Microscopy. Biotechniques *43*, 25–30. https://doi.org/10.2144/000112517.

STAR★METHODS

KEY RESOURCES TABLE

REAGENT or RESOURCE	SOURCE	IDENTIFIER
Antibodies		
rat anti-mCherry	Invitrogen	Cat# M11217; RRID: AB_2536611
goat anti-ChAT	Millipore	Cat# AB144P; RRID: AB_2079751
guinea pig anti-VGLUT2	Millipore	Cat# AB2251; RRID: AB_1587626
goat anti-rat rhodamine	Invitrogen	Cat# 31680; RRID: AB_228357
donkey anti-goat 647	Jackson ImmunoResearch	Cat# 705-605-003; RRID: AB_2340436
goat anti-guinea pig 647	Invitrogen	Cat# A-21450; RRID: AB_2535867
Bacterial and virus strains		
AAV9-CaMKIIa-hChR2(H134R)-EYFP	Addgene; gift from Karl Deisseroth[75]	Viral prep #26969-AAV9; RRID: Addgene_26969
AAV9-CamKII0.4-eGFP-WPRE-rBG	Addgene; gift from James M. Wilson	Viral prep # 105541-AAV9; RRID: Addgene_105541
AAV1-CAG-FLEX-H2B-HA.N2cG	BRAIN Initiative NeuroTools Viral Vector Core, UNC; plasmid was a gift from Thomas Jessell[37]	Addgene plasmid # 73477 ; RRID: Addgene_73477
AAV1-Ef1a-FLEX-TVA-mCherry	BRAIN Initiative NeuroTools Viral Vector Core, UNC; plasmid was a gift from Naoshige Uchida[76]	Addgene plasmid # 38044; RRID: Addgene_38044
RabV CVS-N2c(ΔG)-eGFP	Center for Neuroanatomy with Neurotropic Viruses (P40 OD010996); plasmid was a gift from Thomas Jessell[37]	Addgene plasmid # 73461; RRID: Addgene_73461
Chemicals, peptides, and recombinant proteins		
Tetrodotoxin	HelloBio	HB1034
4-aminopyridine	Sigma	275875
Critical commercial assays		
RNAscope™ Multiplex Fluroescent Reagent Kit v2	ACD Bio	323100
Experimental models: Organisms/strains		
Shox2::Cre mice	Dougherty et al.[3]	MGI:5567920
Gt(ROSA)26Sor$^{tm9/(CAG\text{-}tdTomato)Hze}$/J (Ai9) mice	The Jackson Laboratory	007909
Oligonucleotides		
RNAscope™ Probe, tdTomato	ACD Bio	317041
RNAscope™ Probe, eGFP	ACD Bio	400281-C2
RNAscope™ Probe, Slc17a6	ACD Bio	456751-C3
Software and algorithms		
pClamp 9	Molecular Devices	https://www.moleculardevices.com/products
ImageJ	National Institutes of Health	https://imagej.net/ij/index.html
MATLAB	MathWorks	https://www.mathworks.com/
MATLAB Code for contours	this paper	https://github.com/heyshayna/SinghBrainstemManuscript2025

EXPERIMENTAL MODEL AND STUDY PARTICIPANT DETAILS

All animal experiments were performed using wildtype C57BL/6 and the following transgenic mouse lines: *Shox2::Cre*[3] (*Shox2*$^{tm1.1(cre)Oki}$) and *Ai9(RCL-tdT)*[77] from The Jackson Laboratory (B6.Cg-*Gt(ROSA)26Sor*$^{tm9/(CAG\text{-}tdTomato)Hze}$/J, #007909). Both male and female adult (≥P25) mice were used for this study. Sex differences were not assessed in this study. All experimental procedures followed National Institutes of Health guidelines and were approved by the Institutional Animal Care and Use Committee at Drexel University (LA-23-731). Mice were group housed on a 12 hour light/dark cycle with *ad libitum* access to food and water.

METHOD DETAILS

Surgical procedures

For spinal microinjections, male and female mice (P25-29) were anesthetized with isoflurane (4% induction, 2% maintenance). Dorsal skin was shaved and sterilized with betadine and isopropyl alcohol. After making an incision over lumbar spinal segments, a 1-1.5 segment laminectomy was performed, exposing the dorsal surface of the spinal cord. Four microinjections (500nL per microinjection, two on either side of the midline) of a mixture containing both AAV1-CAG-FLEX-H2B-HA.N2cG and AAV1-Ef1a-FLEX-TVA-mCherry (250nL each per microinjection) were delivered about 0.75mm deep into the spinal cord using a microinjection pump controller (WPI UMC4) and nanoinject II injector (Drummond 3-000-204) via a glass pipette. Following injections, dorsal skin was sutured. Mice received SR buprenorphine analgesic (0.5 mg/kg) and Baytril antibiotic (10 mg/kg) subcutaneously perisurgically. This procedure was repeated 4 weeks later in the same mice but with RabV CVS-N2c(ΔG)-eGFP.[37] CVS-N2c(ΔG) rabies microinjections (250nL each, two on either side of the midline) were delivered with the titer of $\geq 1.59 \times 10^8$ ffu/mL. Mice were perfused 10 days after CVS-N2c(ΔG) rabies injection for anatomy.

For stereotaxic brainstem injections, male and female mice (>P40) were anesthetized with isoflurane (4% induction, 2% maintenance). Scalps were shaved and sterilized with betadine and isopropyl alcohol. Once secured in the stereotaxic frame (Kopf Instruments 900LS), bilateral injections (100nL each) of AAV9-CaMKIIa-hChR2(H134R)-EYFP or AAV9-CamKII0.4-eGFP-WPRE-rBG were delivered using a microinjection pump (WPI NC1987991) into the LPGi (AP -6.96mm, ML ±0.08mm, and DV -5.7 to -6mm). Coordinates were initially taken from the Paxinos atlas of the mouse brain[38] and adjusted mediolaterally following pilot experiments. Following injections, scalps were sutured. Mice received SR buprenorphine analgesic (0.5 mg/kg) and Baytril antibiotic (10 mg/kg) subcutaneously perisurgically. Mice were perfused 3 weeks following injections for anatomy or slices were prepared for electrophysiological recordings 6 weeks following injections.

Immunohistochemistry and RNAscope *in situ* hybridization

Mice were anesthetized with ketamine (150mg/kg) and xylazine (15mg/kg) and perfused transcardially with 0.1M PBS, followed by 4% PFA in PBS. Spinal cords and brainstems were harvested from each animal and fixed overnight in 4% PFA solution at 4°C. Fixed tissue samples were subsequently maintained in 30% sucrose in PBS for at least 48 hours. Tissue was then embedded in OCT compound (Thermo Fisher Scientific) over dry ice and stored at -80°C. Brainstems and lumbar spinal cords were sectioned (20-40μm) transversely on a cryostat (Microm HM 505 E), directly mounted onto charged slides, and stored at -20°C. Slides were washed in PBS before being used for immunohistochemistry or RNAscope.

For immunohistochemistry, slides were first blocked in a PBS solution containing 5% donkey or goat serum, 1% bovine serum albumin, 0.2% Triton X-100, and 0.1% fish gelatin. Slides were incubated overnight in rat anti-mCherry (1:1000, Invitrogen M11217), goat anti-ChAT (1:100, Sigma AB144P), or guinea pig anti-VGLUT2 (1:200, Sigma AB2251). Slides were then incubated for 2 hours in goat anti-rat rhodamine (1:400, Invitrogen 31680), donkey anti-goat 647 secondary antibody (1:400, Jackson ImmunoResearch 705-605-003), or goat anti-guinea pig 647 secondary antibody (1:400, Invitrogen A-21450). All immunohistochemistry steps were performed at room temperature.

RNAscope was performed according to manufacturer's protocols.[78] ACDBio probes used include tdTomato (317041), eGFP (400281-C2), and Slc17a6 (456751-C3). All slides from both immunohistochemistry and RNAscope were coverslipped using Fluoromount-G with DAPI (Invitrogen 00-4959-52). Images were acquired as sequential z stacks of 20x tile-scans on a Leica DM6 fluorescence or Leica SP8 confocal microscope.

Anatomical mapping

RabV-eGFP$^+$ cell bodies in medulla images were counted and marked using the multipoint tool in ImageJ and maps were constructed in Adobe Illustrator. RabV-eGFP$^+$, mCherry$^+$, and RabV-eGFP$^+$/mCherry$^+$ cell bodies in lumbar spinal cord images were counted and marked using the multipoint tool in ImageJ. Marked cell bodies were converted to representative dot maps in Adobe Illustrator. Representative dot maps were used to generate contour isoline figures in MATLAB using a custom script which is available online (https://github.com/heyshayna/SinghBrainstemManuscript2025).

Electrophysiological recordings

To access lumbar spinal Shox2 interneurons in the spinal slice, mice were first anesthetized with ketamine (150mg/kg) and xylazine (15mg/kg). Following decapitation and evisceration, spinal cords were removed from all mice in ice-cold dissecting solution. The dissection solution contained (in mM): 222 glycerol, 3 KCl, 11 glucose, 25 $NaHCO_3$, 1.3 $MgSO_4$, 1.1 KH_2PO_4, and 2.5 $CaCl_2$. The lumbar spinal cord was sectioned transversely (300μm) in dissection solution using a vibrating microtome (Leica Microsystems). Slices were immediately transferred to recording artificial cerebrospinal fluid (ACSF) containing the following (in mM): 111 NaCl, 3 KCl, 11 glucose, 25 $NaHCO_3$, 1.3 $MgSO_4$, 1.1 KH_2PO_4, and 2.5 $CaCl_2$. Slices were incubated at 34-37°C for 30 minutes and then rested at room temperature for 1 hour before recording. Dissecting and recording solutions were continuously aerated with 95%/5% O_2/CO_2.

Fluorescently labeled tdTomato$^+$ Shox2 interneurons were visualized with a 63X objective lens on a BX51WI scope (Olympus) using LED illumination (Lumen Dynamics X-Cite) and targeted for whole cell patch clamp recordings. Electrodes were pulled to tip resistances of 5–12 MΩ using a multi-stage puller (Sutter Instruments) and were filled with intracellular solution which contained

(in mM): 128 K-gluconate, 10 HEPES, 0.0001 $CaCl_2$, 1 glucose, 4 NaCl, 5 ATP, and 0.3 GTP. All recordings were performed at room temperature. Data were collected with a Multiclamp 700B amplifier (Molecular Devices) and Clampex software (pClamp9, Molecular Devices). Signals were digitized at 20kHz and filtered at 6kHz.

Resting membrane potential was recorded shortly after gaining whole-cell access, and neurons with resting membrane potentials more depolarized than -40mV were excluded. To activate channelrhodopsin and record light-evoked postsynaptic currents, neurons were held at -50mV in voltage clamp mode. We delivered 2ms pulses of 0.75-1.5mW blue LED light at 1 Hz through the 63X objective (Lumen Dynamics X-Cite) for 10 seconds per trial. For measurements 5-6 trials were averaged. Latency of excitatory postsynaptic currents was calculated by measuring the time between the beginning of the light stimulation artifact to the beginning of the inward current. Amplitude was measured as the maximum current response. Tetrodotoxin (0.5μM, Hello Bio HB1034) and 4-aminopyridine (100μM, Sigma 275875) were used to isolate monosynaptic light-evoked responses. Both were dissolved in recording ACSF.

QUANTIFICATION AND STATISTICAL ANALYSIS

eGFP RNA^+ cell counting was performed in ImageJ using the Nucleus Counter Plugin,[79] and overlap with VGLUT2 RNA^+ neurons was counted manually using the multipoint tool. Puncta counting was performed manually in ImageJ using the multipoint tool. Cell area measurements were taken manually with freehand selections after adjusting image scale in ImageJ. Measurements of postsynaptic currents were manually calculated from recording traces in Clampfit 11 (Clampex, Molecular Devices). Values reported are means of the first light-evoked response in each trial. Results are reported as mean+/-SD, unless otherwise noted.